communications earth & environment

ARTICLE

https://doi.org/10.1038/s43247-024-01219-8 OPEN

Vertical accretion trends project doughnut-like fragmentation of saltmarshes

Christopher J. Hein[1✉], Jennifer E. Connell[1], Duncan M. FitzGerald[2], Ioannis Y. Georgiou[3], Zoe J. Hughes[2] & Kendall King[1,4]

Coastal saltmarshes keep pace with sea-level rise through in-situ production of organic material and incorporation of allochthonous inorganic sediment. Here we report rates of vertical accretion of 16 new sediment cores collected proximal to platform edges within saltmarshes located behind four barrier islands along the southeast United States coast. All but two of these exceed the contemporaneous rate of relative sea-level rise, often by a factor of 1.5 or more. Comparison with 80 additional measurements compiled across the Georgia Bight reveals that marshes situated closer to inlets and large bays generally accrete faster than those adjacent to small creeks or within platform interiors. These results demonstrate a spatial dichotomy in the resilience of backbarrier saltmarshes: marsh interiors are near a tipping point, but allochthonous mineral sediment fluxes allow enhanced local resilience along well-exposed and platform-edge marshes. Together, this suggests that backbarrier marshes are trending towards rapid, doughnut-like fragmentation.

[1] Virginia Institute of Marine Science, William & Mary, Gloucester Point, VA, USA. [2] Department of Earth and Environment, Boston University, Boston, MA, USA. [3] The Water Institute, New Orleans, LA, USA. [4] Department of Geology, William & Mary, Williamsburg, VA, USA. ✉email: hein@vims.edu

The sustainability of coastal saltmarshes in the face of moderate rates of sea-level rise relies on the combined ability of these wetlands to migrate upland and/or retain vertical elevation with respect to the tidal frame[1]. The latter is achieved through belowground production and preservation of organic material and surficial deposition of inorganic sediment[2,3]. Estimates of marsh accretion potential based on both process-based numerical modeling and field studies from marshes across latitudes and tidal range suggest that marshes with high rates of organic production or inorganic sediment delivery are capable of maintaining their elevation even at relatively high rates of relative sea-level rise (RSLR) (e.g., refs. [4–8]). This reflects the enhanced sediment-trapping ability of marsh plants when exposed to greater depths and duration of inundation[9,10]; greater root productivity at higher temperature and CO_2 levels[11,12]; higher rates of sediment and nutrient delivery resulting from increased storminess[13–15]; and enhancement of pore space in organic-rich marshes[16].

However, saltmarsh responses to changing climatic and anthropogenic conditions are not uniformly positive: mineral sediment availability remains broadly limited, especially along high-latitude, formerly glaciated coasts[17,18]; warming may lead to accelerated decomposition of belowground biomass and decreased allocation of biomass to marsh root systems, particularly in higher-latitude marshes[19]; and the same storms that can provide fresh sediment and nutrients can also induce vegetation die-off, plant removal, pond formation, peat decomposition, soil shrinkage, subsidence, and increased standing water[20,21]. Such observations have led many authors to conclude that the ability of saltmarshes to maintain elevation with respect to the tidal frame is threatened, if not already faltering (e.g., refs. [6,9,18,22,23]).

Given the importance of sediment availability for marsh resilience (e.g., refs. [6,24]), it is expected that only those saltmarshes benefitting from high sediment inputs will be capable of withstanding the predicted acceleration in sea-level rise over the coming decades. Indeed, studies that attempt to account for differences in sediment availability and the rate of RSLR through latitudinal or global compilations have demonstrated marsh resilience in the form of accelerating accretion in response to sea-level rise, in part through increasing sediment delivery even in sediment-poor systems[8,23]. However, modeling studies and large-scale comparisons often cannot account for the very local (sub-kilometer-scale) processes responsible for delivering sediment to the marsh surface, and thus fail to capture the nuances responsible for controlling marsh accretion in field settings.

Here we focus on barrier-associated marshes of the 'Georgia Bight' (southeast USA states of South Carolina [SC], Georgia [GA], and Florida [FL]; Fig. 1, left pane). While the well-studied, microtidal, deltaic marshes of the USA Gulf Coast are commonly located proximal to shallow, expansive open-water bays, where mud is readily resuspended and moved onshore by storm surges, marshes along the USA South Atlantic coast are fronted by wide barrier islands. These constrict storm surge via narrow tidal inlets and protect marshes from open-ocean waves, resulting in only locally generated, limited-fetch waves, except proximal to tidal inlets. The mixed-energy barrier systems of the Georgia Bight are fed only by moderate-sized rivers discharging to the nearby coast, rather than into the marsh system. The associated backbarrier marshes are 5–7 km wide, contain relatively coarse inorganic sediment (sand:mud ratios of 0.2–0.5; see Supplementary Table 1) as compared with deltaic marshes, and experience RSLR rates that are ~1.5–2.0 times the global average (Supplementary Table 1). However, these barrier-marsh systems diverge latitudinally in terms of relative wave and tidal influence[25], with spring range varying by ~1 m. Thus, they can serve as a proxy for mesotidal, barrier-associated marshes across a range of settings.

Previous estimates of marsh accretion and sedimentation rates from the Georgia Bight are generally from marsh interiors, distal to large bodies of water and associated inorganic sediment sources. In contrast, we present new accretion rates derived from analysis of short-lived radioisotopes from 16 cores collected near marsh edges along mainland-to-barrier transects behind four of these island systems (Cape Romain, SC; Hilton Head, SC; Sapelo Island, GA; Amelia Island, FL) (Fig. 1). Backbarrier marshes at all sites are dominated by *Spartina alterniflora* with *Spartina pumilus* (formerly *Spartina patens*) prevalent at higher elevations. These platform marshes are dissected by tidal channels which vary from creeks several meters in width to bays several kilometers across. The latter include Sapelo and Doboy Sounds, which delimit the marshes of Sapelo Island, and Calibogue and Port Royal Sounds, abutting those of Hilton Head. New accretion rates are derived from sites within the marshes representing a range of exposures to open-water conditions. We then compare our newly derived rates to a regional (Georgia Bight) database of accretion and/or surface elevation-change estimates compiled from estimates based on excess radioactive lead ($^{210}Pb_{xs}$), radioactive cesium (^{137}Cs), Surface Elevation Tables (SET), and Marker Horizons (MH). We find that, in general, marshes proximal to creek margins and open water bodies have accreted at or faster than RSLR, with the most vertically resilient barrier-associated marshes located at sites with the greatest exposure to open bays and tidal inlets.

Results and discussion

Rapid accretion of marsh edges in the Georgia Bight. Summary sedimentologic and accretion data for each of our 16 new marsh accretion cores are reported in Table 1 and constant flux with constant sedimentation (CFCS) accretion rate ($^{210}Pb_{xs}$CFCS) values are shown spatially in Fig. 1. Example down-core ^{210}Pb, ^{137}Cs, bulk density, and loss-on-ignition profiles are shown in Fig. 2; full down-core data are provided in Supplementary Figs. 1–4. Additional data are provided in Supplementary Data 1, including the parameters used to define dimensionless parameters: 1) AE_C (Contemporaneous Accretion Excess), which is the measured, site-specific accretion rate divided by RSLR during the period of record ($RSLR_C$), and 2) AE_{50} (50-year Accretion Excess), defined as the site-specific accretion rate divided by the rate of RSLR during the 50 years prior to sampling ($RSLR_{50}$) (see Methods for details and example calculations).

Our $^{210}Pb_{xs}$CFCS accretion rates range from 1.91 ± 0.07 mm yr^{-1} (HH-T2S2) to 13.91 ± 0.07 mm yr^{-1} (SI-T2S2), with a mean rate (±S.D.) of 6.29 ± 0.18 mm yr^{-1}. We find greater variability in marsh accretion within each barrier system (average range: 7.80 mm yr^{-1}) than between systems (range of system averages: 2.73 mm yr^{-1}). The resulting AE_C values range from 0.6 ± 0.1 (HH-T2S4) to 4.9 ± 0.5 (AI-T1S3). This latter marsh sampling station, with a $^{210}Pb_{xs}$CFCS accretion rate of ~12.5 mm yr^{-1}, shows weak correspondence to its associated ^{137}Cs rate (~5.9 mm yr^{-1}), and an AE_C value of nearly double that of the next highest station (SI-T2S2; $AE_C = 2.58 \pm 1.2$). Although loss-on-ignition and bulk density values for this core are not dissimilar from our other sampling stations (Table 1), the presence of surface samples (0–4 cm) low in ^{210}Pb activity (see Supplementary Fig. 3; note that these samples are omitted from $^{210}Pb_{xs}$CFCS analysis) indicates possible reworking or event deposition. We thus treat it as an outlier. With this sample removed, we find moderately strong agreement ($r^2 = 0.81$; $p \ll 0.01$) between $^{210}Pb_{xs}$CFCS rates and those determined from peak ^{137}Cs (Supplementary Fig. 5a), which increases our confidence in the $^{210}Pb_{xs}$CFCS values.

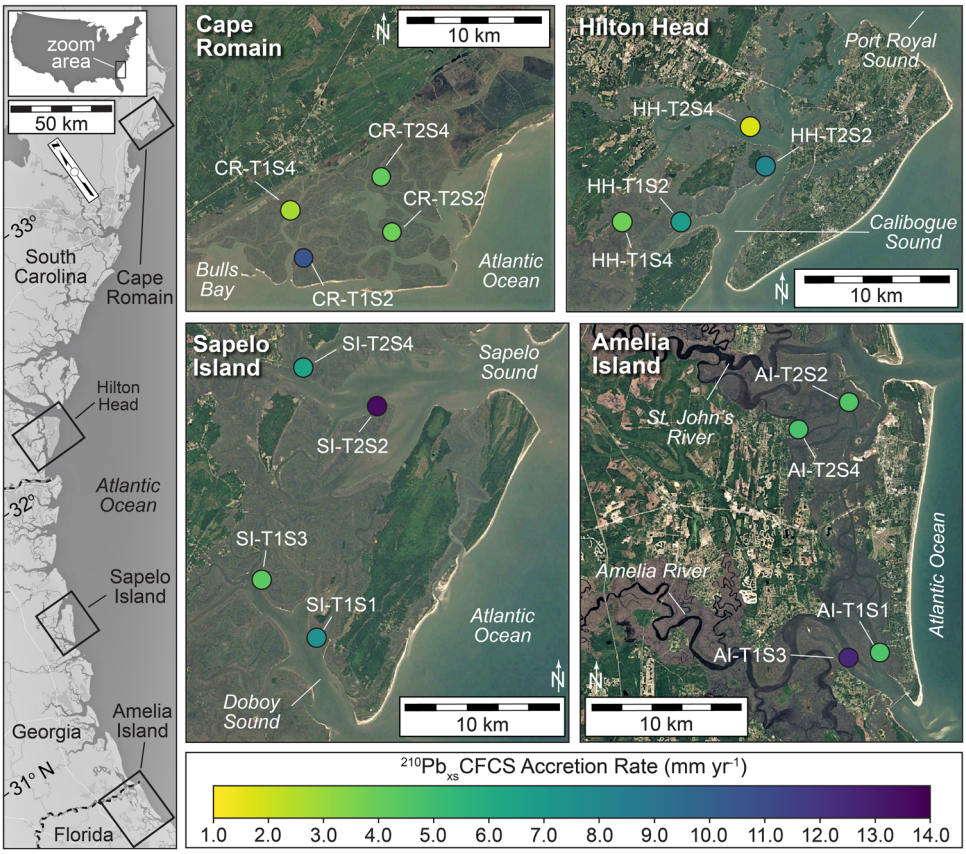

Fig. 1 Barrier-associated marsh sampling stations and calculated accretion rates. Locations sampled for determination of new marsh accretion rates. These are located behind four mixed-energy barrier systems along the Georgia Bight of the southeast USA coast. Core locations are shown as circles, color-coded by calculated $^{210}Pb_{xs}$CFCS accretion rate. Core IDs are given as site name (e.g., CR = Cape Romain), mainland-to-barrier transect ID (e.g., "T1"), and station number (e.g., "S4"). Satellite imagery: Google, ©2020 Landsat/Copernicus.

Table 1 Summary of results.

Core identification	Latitude	Longitude	Elevation (m MTL [2022])	$LOI_{Pb\text{-}xs}$ (%)	$BD_{Pb\text{-}xs}$ (g cm^{-3})	$^{210}Pb_{xs}$CFCS Accretion Rate (mm yr^{-1})	^{137}Cs Accretion Rate (mm yr^{-1})	AE_C	AE_{50}
CR-T1S2	33.032527	−79.469664	0.62 ± 0.02	18.9 ± 0.8	0.42 ± 0.03	10.62 ± 0.56	8.78 ± 0.52	2.60 ± 0.73	3.12 ± 0.59
CR-T1S4	33.058954	−79.467841	0.31 ± 0.02	14.0 ± 1.8	0.51 ± 0.10	2.72 ± 0.03	2.37 ± 0.24	0.80 ± 0.08	0.80 ± 0.19
CR-T2S2	33.041353	−79.406222	0.53 ± 0.02	19.8 ± 2.3	0.44 ± 0.05	3.96 ± 0.04	2.67 ± 0.19	1.27 ± 0.13	1.16 ± 0.20
CR-T2S4	33.075647	−79.414808	0.61 ± 0.02	22.8 ± 2.2	0.37 ± 0.05	4.16 ± 0.02	3.70 ± 0.15	1.32 ± 0.12	1.22 ± 0.19
HH-T1S2	32.149976	−80.855494	0.63 ± 0.02	15.5 ± 0.8	0.36 ± 0.04	6.85 ± 0.23	4.89 ± 0.19	1.85 ± 0.29	1.87 ± 0.31
HH-T1S4	32.154059	−80.902741	0.86 ± 0.02	21.4 ± 2.8	0.36 ± 0.03	3.91 ± 0.12	4.44 ± 0.17	1.23 ± 0.16	1.07 ± 0.24
HH-T2S2	32.182787	−80.797581	0.97 ± 0.02	10.6 ± 1.5	0.69 ± 0.11	8.17 ± 0.39	8.85 ± 0.48	2.01 ± 0.50	2.23 ± 0.44
HH-T2S4	32.204931	−80.812619	0.48 ± 0.02	13.8 ± 0.4	0.47 ± 0.11	1.91 ± 0.07	2.17 ± 0.19	0.64 ± 0.11	0.52 ± 0.22
SI-T1S1	31.416838	−81.300181	0.98 ± 0.02	22.5 ± 2.0	0.39 ± 0.09	7.33 ± 0.55	4.63 ± 0.20	2.15 ± 0.71	2.33 ± 0.62
SI-T1S3	31.446392	−81.337780	0.78 ± 0.02	21.6 ± 2.8	0.33 ± 0.04	4.20 ± 0.07	2.59 ± 0.22	1.29 ± 0.36	1.34 ± 0.30
SI-T2S2	31.531204	−81.270948	0.82 ± 0.02	15.2 ± 2.3	0.50 ± 0.08	13.43 ± 0.43	n/a	2.58 ± 1.20	4.27 ± 0.52
SI-T2S4	31.544052	−81.310322	0.69 ± 0.02	14.5 ± 2.0	0.51 ± 0.06	6.80 ± 0.14	5.56 ± 0.20	2.20 ± 0.38	2.16 ± 0.33
AI-T1S1	30.546145	−81.464970	0.55 ± 0.02	17.4 ± 3.2	0.43 ± 0.07	4.70 ± 0.05	2.72 ± 0.17	1.84 ± 0.15	1.79 ± 0.22
AI-T1S3	30.539876	−81.481510	0.48 ± 0.02	22.1 ± 3.0	0.34 ± 0.05	12.45 ± 0.26	5.94 ± 0.46	4.91 ± 0.50	4.74 ± 0.33
AI-T2S2	30.690916	−81.484537	0.53 ± 0.02	27.4 ± 3.4	0.33 ± 0.05	4.63 ± 0.10	3.07 ± 0.19	1.80 ± 0.18	1.76 ± 0.23
AI-T2S4	30.676519	−81.515868	0.36 ± 0.02	30.9 ± 2.7	0.23 ± 0.03	4.81 ± 0.34	3.85 ± 0.19	1.80 ± 0.42	1.83 ± 0.40

$LOI_{Pb\text{-}xs}$ and $BD_{Pb\text{-}xs}$ values are means (weighted by sample thickness) ± std. dev. of the loss-on-ignition and bulk density, respectively, values of core samples used to determine $^{210}Pb_{xs}$CFCS for a given core. Error values for $^{210}Pb_{xs}$CFCS and ^{137}Cs accretion rates and AE_C and AE_{50} values are methodological uncertainties (or propagation thereof), as described in Methods. Core identifiers are given as site name (CR = Cape Romain, South Carolina; HH = Hilton Head, South Carolina; SI = Sapelo Island, Georgia; AI = Amelia Island, Florida), mainland-to-barrier transect ID (e.g., "T1"), and station number (e.g., "S4"). m MTL = meters above local mean tidal level; SLR_C = contemporaneous relative sea-level rise rate; AE_C = contemporaneous accretion excess ($^{210}Pb_{xs}$CFCS/$RSLR_C$); AE_{50} = 50-year accretion excess ($^{210}Pb_{xs}$CFCS/$RSLR_{50}$).

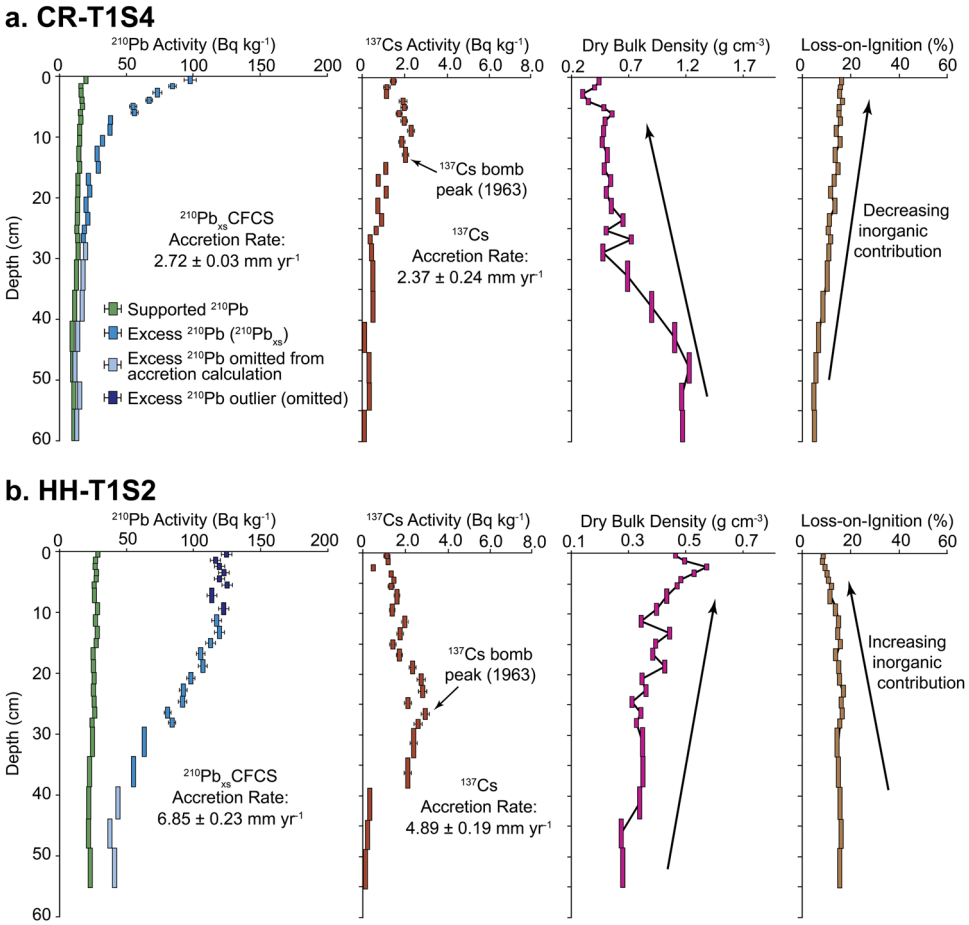

Fig. 2 Representative examples of marsh core profiles. Representative examples of down-core ^{210}Pb, ^{137}Cs, bulk density, and loss-on-ignition profiles for (**a**) slowly (Cape Romain station CR-T1S4) and (**b**) rapidly (Hilton Head station HH-T1S2) accreting marshes. Profiles for the full set of cores are given in Supplementary Fig. 1 (Amelia Island stations), S2 (Sapelo Island stations), S3 (Hilton Head stations), and S4 (Cape Romain stations). Error bars on individual ^{210}Pb and ^{137}Cs data points are instrumental measurement uncertainty.

Our results indicate that marsh accretion at 14 of our 16 stations, all positioned ~10 m in from the platform edge, outpaced RSLR over the same period ($AE_C > 1$); in fact, a mean AE_C value for our 16 stations of 1.9 ± 0.3 indicates that these marshes are (on average) accreting at a pace nearly twice that of $RLSR_C$. Within each barrier system, our marsh stations are also accreting at mean rates between 1.4 ± 0.3 (Sapelo Island) and 2.6 ± 0.2 (Amelia Island) times the rate of contemporaneous RSLR. Compared to longer-term sea-level records, we likewise find that marsh accretion outpaces $RSLR_{50}$ ($AE_{50} > 1$) at all but two of our sampled stations (HH-T2S4 and CR-T1S4; the same two with AE_C values < 1). Mean AE_{50} values for all barrier systems was 2.0 ± 0.1, modestly higher than corresponding AE_C values. Mean AE_{50} values within sites range from 1.4 ± 0.9 (Hilton Head) to 2.5 ± 0.1 (Sapelo Island). The similarities between our calculated AE_C and AE_{50} values are expected given the robust period of record captured by our $^{210}Pb_{xs}$CFCS method (mean: 53.3 years).

We find that higher rates of marsh accretion correspond with higher elevations within the tidal frame: tide-range-normalized elevation (Z^*_{MHW} values) can explain ~20% of the variance in $^{210}Pb_{xs}$CFCS rates ($r^2 = 0.26$; $p < 0.1$; Supplementary Fig. 5b), AE_C ($r^2 = 0.21$; $p < 0.1$), and AE_{50} ($r^2 = 0.19$; $p \sim 0.1$). This outcome is aligned with that of Langston et al. [26] for the Sapelo Island marshes. However, it is contradictory to the expected, well-established negative relationship between elevation and marsh accretion; i.e., marshes situated lower in the tidal frame experience a greater hydroperiod and, as a result, should accrete faster due to higher inorganic sediment inputs and organic matter accumulation (e.g., ref. [9]). We posit that this finding likely reflects the narrow elevation range of the marsh platform with respect to tidal range, and thus the limited range of elevations captured by our cores (~68 cm).

Among our 16 cores, mean (±1 std. dev.) bulk density and loss-on-ignition values across the same core depths used to calculate $^{210}Pb_{xs}$CFCS rates ('$BD_{Pb\text{-}xs}$' and '$LOI_{Pb\text{-}xs}$') are 0.42 ± 0.03 g cm^{-3} and 19.3 ± 0.9%, respectively. The lowest bulk density and highest loss-on-ignition values (0.23 ± 0.03 g cm^{-3} and 31 ± 2.7%, respectively) are found in core AI-T2S4 and the highest bulk density and lowest loss-on-ignition values (0.69 ± 0.11 g cm^{-3} and 11 ± 1.5%, respectively) are from core CR-T1S4. We find no correlation between AE_C and either $BD_{Pb\text{-}xs}$ ($r^2 < 0.01$; $p > 0.50$; Supplementary Fig. 5c) or $LOI_{Pb\text{-}xs}$ ($r^2 = 0.02$; $p = \sim 1.0$; Supplementary Fig. 5d); correlations with AE_{50} values are even weaker. Comparisons with $^{210}Pb_{xs}$CFCS accretion rates reveal only very weak positive (bulk density; $r^2 = 0.03$; $p \sim 0.50$) and very weak negative (loss-on-ignition; $r^2 = 0.02$; $p > 0.50$) relationships. Multiple linear regressions of combinations of Z^*_{MHW}, $BD_{Pb\text{-}xs}$, and $LOI_{Pb\text{-}xs}$ against $^{210}Pb_{xs}$CFCS accretion rates, AE_C, and AE_{50} values reveal similarly insignificant to nonexistent correlations.

Regional comparison reveals that Georgia Bight marshes overall are threatened by recent acceleration in sea-level rise.

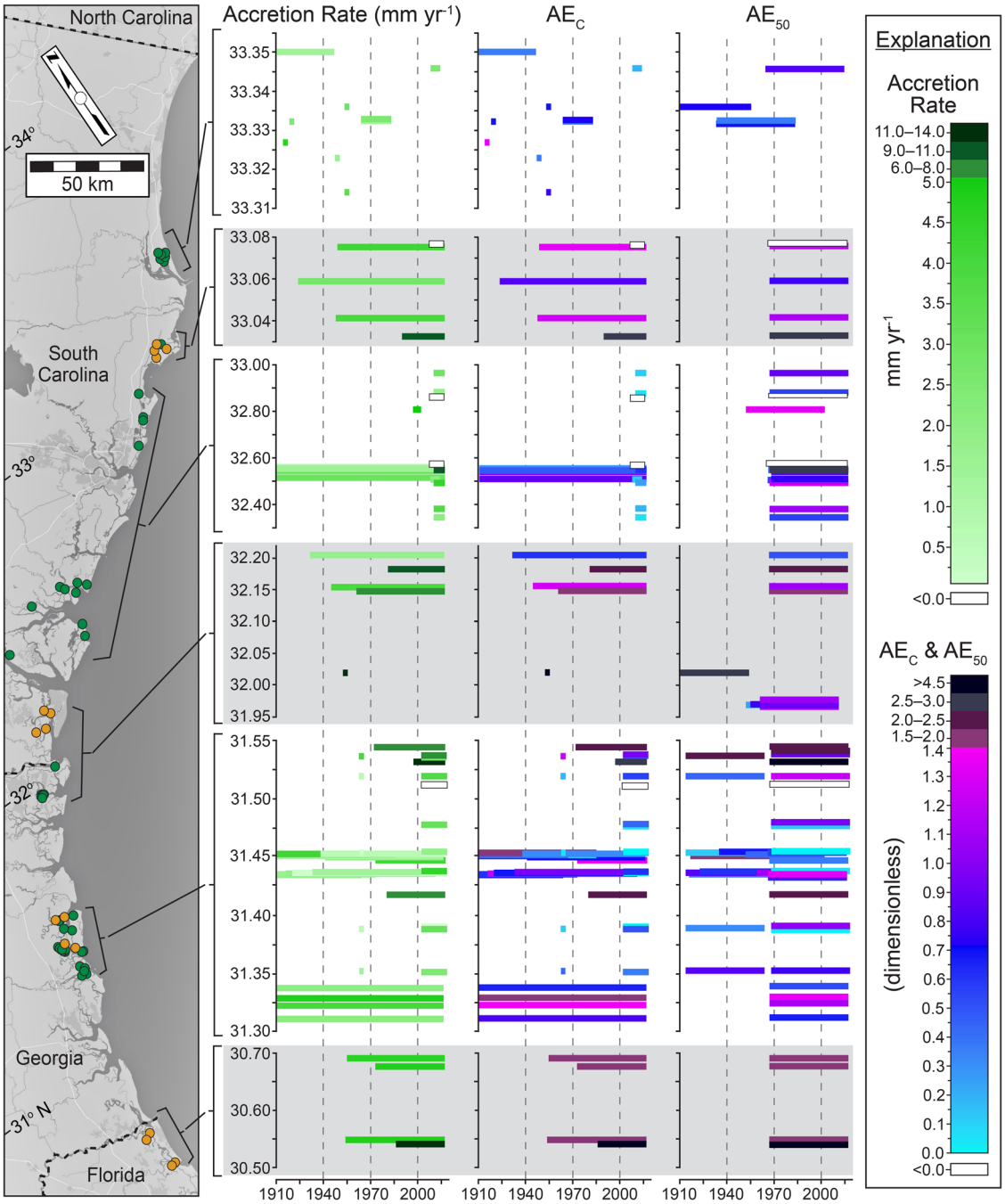

Fig. 3 Latitudinal gradients in marsh accretion across the USA Georgia Bight. Accretion-rate, AE_C, and AE_{50} values for marshes from the southeast USA Atlantic Coast. Data are plotted by latitude (*y*-axis). Bar widths correspond to the period, in years C.E. (*x*-axis), captured by the analysis. Core locations are shown in green (this study: gold) circles on the map. Records which end prior to 1950 are omitted because of uncertainty in AE_{50} values due to incomplete relative sea-level records. See Supplementary Data 1 for details and data sources.

Incorporating data from our new cores into a regional database for the Georgia Bight (Supplementary Data 1), we find no large-scale spatial trends in accretion rates, AE_C, nor AE_{50} values (Fig. 3), despite regional variation in spring tidal range of ~1 m. Furthermore, as with our new cores, the regional database shows no significant correlations between Z^*_{MHW} and any of marsh accretion rate (Supplementary Fig. 6a), AE_C values (Supplementary Fig. 6b), or AE_{50} values (Supplementary Fig. 6c).

Plotting calculated and reported accretion rates against associated $RSLR_C$ and $RSLR_{50}$ rates (Fig. 4) reveals the potential resilience of these marshes to accelerated RSLR and their ability to equilibrate to higher rates of rise over several decades: generally, accretion rates show a better comparison (plot above or closer to the 1:1 line) to the 50-year sea-level rise rate. This reflects the partial dependence of calculated rates of vertical accretion (or estimates of 'surface elevation change' in the case of SETs or sedimentation in the case of MHs) on the observational timescale, in part because shorter records tend to preferentially incorporate more of the late 20th–early 21st century acceleration in global sea-level rise[27]. For example, we find that, generally, the short-term MH-derived (average record length: 14.1 years) and ^{137}Cs-derived (average record length: 32.5 years) accretion records have AE_{50} values (mean: 1.10 [MH] and 0.76 [^{137}Cs]) which are ~2 times higher than associated AE_C

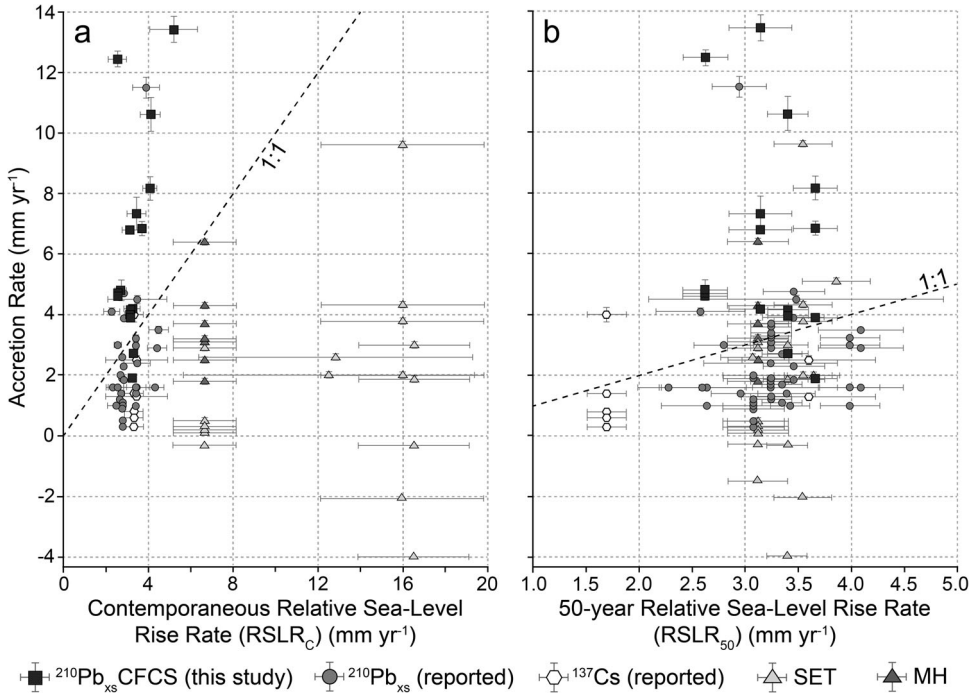

Fig. 4 Trends in marsh accretion as a function of relative sea-level rise. Comparisons between marsh accretion rates and local relative sea-level rise rates (±S.D.) for (**a**) the period contemporaneous with which accretion was calculated ($RSLR_C$); and for (**b**) the 50-year period prior to the sampling date (or end of the measurement period for SETs) ($RSLR_{50}$).

values from those same records (mean: 0.54 [MH] and 0.46 [^{137}Cs]). No such difference exists for accretion rates determined through the longer-term ^{210}Pb method (average record length: 74.3 years; mean $AE_{50} = 1.06$; mean $AE_C = 1.15$); this observation holds even after removal of our new, relatively high, accretion rates (average record length: 83.6 years; mean $AE_{50} = 0.73$; mean $AE_C = 0.78$). Moreover, the observed trend in low AE_C values derived from SET and MH measurements shifts considerably when comparing those accretion rates to $RSLR_{50}$ (Fig. 4b): eight of these 25 SET/MH records have AE_{50} values > 1, whereas none show $AE_C > 1$. Accretion rates calculated via both ^{210}Pb and ^{137}Cs also show a similar, if less dramatic, shift towards higher degrees of resilience (as captured by higher AE_{50} values). The reason for this is simple: in comparing accretion rates to $RSLR_{50}$, the resulting AE_{50} values tend to be higher, on average, because they are calculated for a longer period of RSLR (50 years in all cases), whereas AE_C values normalize accretion by a shorter period (especially for SET/MH measurements). Whether this portends enhanced marsh resilience over the longer term remains an unanswered question, but provides additional support for the careful consideration of the role of response lags in considering the long-term viability of marshes to accelerated RSLR. Moreover, it demonstrates that our AE_{50} values are generally a more conservative estimate of marsh resilience. This is reflected in the "purple shift" between AE_C and AE_{50} values shown in Fig. 3: that is, AE_{50} values are generally higher than corresponding AE_C values, the latter of which generally incorporate a shorter and more recent time period characterized by higher rates of RSLR.

Overall, we calculate a mean AE_{50} value for all new and published data for the Georgia Bight of 0.94 ± 0.16. This indicates that—assuming marshes respond to an increase in the rate of RSLR through more than just an instantaneous response to increased hydroperiod (i.e., that marsh response to RSLR acceleration is lagged by an order of decades)—marshes throughout the Georgia Bight are growing nearly vertically apace with RSLR, in general. However, substantially tempering this observation is the fact that mean AE_{50} for the Georgia Bight marshes falls to only 0.72 ± 0.17 with removal of our 16 new calculated rates; in fact, with the exception of those from our new sediment cores, ~75% of accretion measurements result in AE_{50} values of <1. Most marshes are accreting at an average of only ~50% of the coincident rate of RSLR, or, at most, ~80% of the long-term (50-year) RSLR rate. This clearly suggests that Georgia Bight marshes overall are failing to keep pace with RSLR.

Higher accretion observed at high-exposure marshes. Marshes exposed to large fetches are threatened by edge erosion by waves; yet, where fine sediment is in abundance (e.g., deltaic marshes, such as those in the Mississippi River Delta), those same waves can deliver abundant sediment to the marsh surface, potentially increasing vertical accretion[28,29]. Our findings reveal the same trend for sandier, barrier-associated Georgia Bight marshes: at all four of our sampled barrier systems, marshes located closest to open bodies of water, particularly those adjacent to tidal inlets (e.g., SI-T2S2, which is exposed to Sapelo Sound and Sapelo Inlet, GA; Fig. 1), display the highest rates of accretion (Fig. 1; Table 1), as well as the highest values for AE_C and AE_{50} (Table 1). Removal from barrier-system averages of only the most exposed sampling stations from each of our four barriers (corresponding to the stations from each barrier system with the highest accretion rates) decreases the mean AE_C and AE_{50} values of our new stations from 1.89 and 2.01, to 1.48 and 1.49, respectively. Though still well above other regional accretion rates calculated from ^{210}Pb (0.78 and 0.73 for AE_C and AE_{50}, respectively), this shows the outsized impact of these high-end values on our barrier-system averages. Moreover, our marsh sites located adjacent to only relatively small tidal channels (e.g., stations HH-T2S4 and CR-T1S4) show far lower rates of accretion, and in fact have AE_C and AE_{50} values of <1.0.

The dichotomy between our rapidly accreting, high-exposure marshes and the relatively slow accretion observed at our more

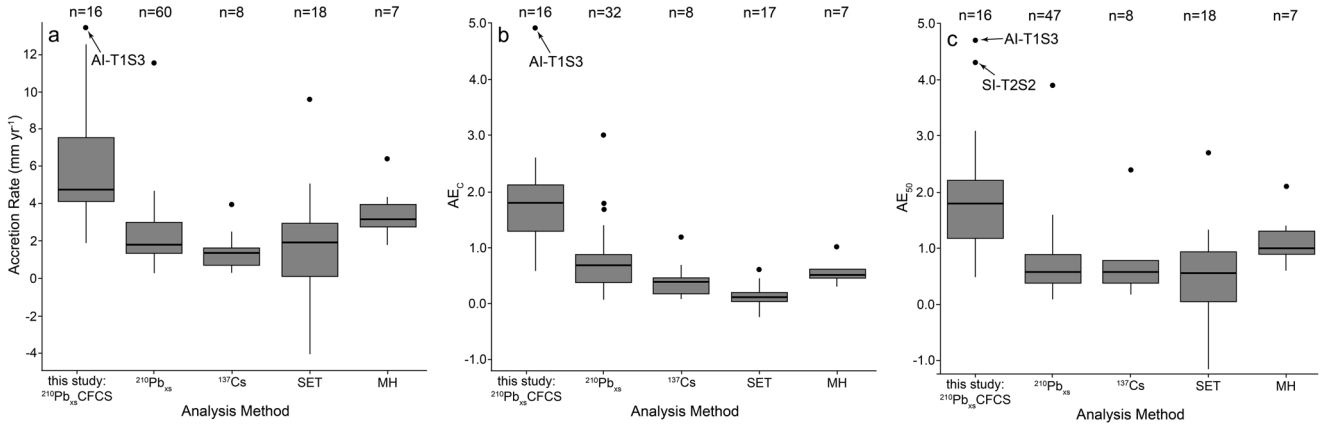

Fig. 5 Methodological comparison of marsh-accretion and sediment-accumulation rates. Box plots (center line, median; box limits, upper and lower quartiles; whiskers, 1.5x interquartile range; points, outliers) of (**a**) accretion rate, **b** AE_C values, and (**c**) AE_{50} values for marshes throughout the Georgia Bight, separated by analysis method. New $^{210}Pb_{xs}$CFCS accretion rates are separated from those reported in the literature (Supplementary Data 1).

interior sites likely reflects the relative exposure of those marshes to hydrodynamic forcings, including wave-induced suspension, and thus the relative ease of delivering sediment to marsh edges well-exposed to wave and tidal processes. For example, the station with our highest calculated $^{210}Pb_{xs}$CFCS accretion rate (SI-T2S2: 13.43 ± 0.43 mm yr^{-1}) is located 8 km from the mouth of Sapelo Sound Inlet (~3 km wide), but where the main channel is still 2.0 km wide and well-exposed to open-ocean conditions, especially during storms (Fig. 1). A similar trend can be seen at station SI-T1S1 ($^{210}Pb_{xs}$CFCS accretion rate: 7.33 ± 0.55 mm yr^{-1}) which is sited only ~5.0 km from the entrance to Doboy Sound Inlet (1.5 km wide) where the channel is still 1.5 km wide.

Likewise, the marsh stations recording the fastest accretion rates at Hilton Head (SC) face Calibogue Sound Inlet (HH-T2S2: 8.17 ± 0.39 mm yr^{-1}) and are along the wide main channels of Calibogue Sound (HH-T1S2: 6.85 ± 0.23 mm yr^{-1}) (Fig. 1). At Cape Romain (SC), we record the highest accretion rates ($^{210}Pb_{xs}$CFCS accretion rate: 10.62 ± 0.56 mm yr^{-1}) at the station (CR-T1S2) closest to the entrance to Five Fathom Creek from Bulls Bay. Amelia Island (FL), however, presents a somewhat different case. Here, measured $^{210}Pb_{xs}$CFCS accretion rates are similar (4.63–4.81 mm yr^{-1}), with the exception of AI-T1S3 (12.45 ± 0.26 mm yr^{-1}). Though this is the most exposed of our four sampling stations within the Amelia Island backbarrier (AI-T1S3 is located along a main channel of the South Amelia River), the anonymously high $^{210}Pb_{xs}$CFCS rate and associated mismatch with our calculated ^{137}Cs rate (5.94 ± 0.46 mm yr^{-1}; also, the highest ^{137}Cs rate for Amelia Island), leave the value for this station in doubt, thus its exclusion from the full analysis.

Nonetheless, a consistent trend emerges: within a set of 16 marsh stations experiencing faster-than-average long-term accretion rates overall, areas experiencing the fastest accretion are found in locations with high wave and storm exposure. In contrast, our sampling stations located centrally within backbarrier marshes, and/or adjacent to smaller creeks commonly have the lowest rates of accretion (and, correspondingly, AE_C and AE_{50} values) (Fig. 1).

Comparing calculated and reported accretion rates to associated $RSLR_C$ and $RSLR_{50}$ rates (Fig. 4) and boxplots of accretion rate, AE_C, and AE_{50} values grouped by analysis method (Fig. 5), we find that 14 of our 16 new marsh accretion rates are significantly ($p \leq 0.0001$, AnOVa; for both AE_C and AE_{50}) faster than other records from the area according to either contemporaneous or 50-year-mean RSLR rates, regardless of how those were determined. A central difference: the vast majority of these previously reported rates are from marsh platform interiors (Supplementary Data 1). Only some stations from Weston et al. [8] report on accretion from near platform edges (~50 m inboard). Though sampled from within the sediment-rich mouths of the Altamaha and Edisto rivers, and determined through similar $^{210}Pb_{xs}$ methods, the resulting accretion rates (avg: ~2.7 mm yr^{-1}) are less than half those determined for our sites (avg: ~6.3 mm yr^{-1}). Also, their rates are generally lower than local RSLR over the contemporaneous period (avg AE_C: 0.9) or the 50 years prior to collection (avg AE_{50}: 0.7). Though marshes at both sites show multi-decadal acceleration in accretion, they are situated within estuaries, with all but one coring site located > 5 km from the river mouth. Importantly, these cores are situated ~40 m further inboard from marsh edges than ours, likely substantially reducing sediment delivery due to the rapid decay in sediment loads with distance inboard of the platform edge (e.g., refs. [30,31]).

Contributions of allochthonous mineral sediments have clear and well-demonstrated benefits to marsh resilience. These sediments can increase surface elevation, provide stress-reducing nutrients to the soil, and reduce phytotoxicity (e.g., refs. [13,14,32]). Further, rates of autocompaction within these sediment-rich peats are generally lower than for comparable organic-rich soils[33], allowing for overall faster vertical growth. Though we find no clear relationship between accretion and inorganic composition of our sampled marshes (Supplementary Figs. 5c, d), we do note that a number of our stations exhibiting most rapid accretion appear to have a higher bulk density and lower loss-on-ignition values (i.e., greater inorganic sediment contributions) near the marsh surface, whereas those with slower accretion commonly show the opposite (Fig. 2; see Supplementary Figs. 1–4 for full data). We find our stations with the greatest exposure to wave energy correspond to those areas with the highest vertical accretion, likely because they receive the highest rates of mineral sediment influx.

Sediment transported to the marsh surface can originate from erosion of proximal lagoon floors[34], mud flats[35], and marsh edges[36]; or be transported into the backbarrier via tidal inlets, particularly during storms (e.g., ref. [37]). These processes appear to be important at several of our bay-facing and/or inlet-proximal sampling locations (e.g., stations AI-T1S3, SI-T1S1, SI-T2S2, and CR-T1S2), where the measured accretion rates are highest. In fact, these same marsh sampling stations contain abundant evidence of recent surficial mineral-dominated storm deposits[38], likely contributing to a well-mixed layer observed in the upper few centimeters in several of our cores (N.B. these layers were

omitted from accretion calculations) (Supplementary Figs. 1–4). These fastest-accreting marshes are also among our highest-elevation sites (with respect to local mean tidal level) (Supplementary Fig. 5b), with our four fastest-accreting marshes located nearly 20 cm higher in elevation than our four slowest-accreting sites. The fact that they have gained elevation at rates faster than long-term RSLR without becoming supratidal may be related to marsh-edge soil-creep processes, such as those observed in New England marshes[39]. The associated steady-state recycling of these near-edge sediments through storm waves and surges (and associated high-water levels) back to the marsh surface may explain the observed and unexpected (weakly) positive correlation between tide-normalized elevation and accretion (Supplementary Fig. 5b).

Implications for marsh resilience to sea-level rise. Fluvial sediment availability and the ability of waves to entrain, and currents to transfer, that sediment to the marsh surface are among the most important contributors to long-term marsh sustainability (e.g., refs. [9,24,29,40]). For example, modeling[6] suggests that marshes located in systems characterized by suspended sediment concentrations of <20 mg L^{-1} may drown at RSLR rates as low as 5 mm yr^{-1}; indeed, recent field studies have substantiated that such sediment-starved marshes are faltering[8,18]. Our results indicate that, even in the relatively sediment-rich backbarrier systems of the southeast USA coast, platform marshes may diverge spatially in their long-term ability to keep pace with RSLR, with differences based largely on the location of those marshes within the backbarrier, or of marsh within the platform. These differences appear magnified even at relatively fine scales (10 s of meters). This finding highlights that the position of an area of marsh within the platform, and the specific platform site within the broader backbarrier setting with respect to wave energy (particularly that coincident with storm surge), play central roles in marsh accretion. As such, we find that leading factors in marsh resilience in backbarrier marshes are associated with the inter- and intra-system characteristics of a given marsh, such as the availability of sediment in adjacent habitats (e.g., mudflats vs rocky reefs) or the patchiness of the marsh, and attendant implications for available fetch and percentage of interior vs. edge habitats[41]. Furthermore, our findings demonstrate that spatially discrete sampling across a range of environments within diverse backbarrier settings are required to ensure complex spatial differences in marsh resilience are fully captured.

We find that marshes located near the periphery of platforms, but still inboard of levees, predominantly record multi-decadal accretion at rates of ~1.5–2.0 times that of RSLR over the coincident time period; and those facing wide bays and/or adjacent to tidal inlets have been accreting even faster (as high as > 4.0 times RSLR in one case). In fact, the only apparent threat to the survival of these marshes is cannibalistic edge erosion, as fronting bays (a source for sediment reaching the marsh surface) deepen, allowing for larger waves to reach the marsh edge[42,43]. In contrast, low-exposure and platform-interior marshes are generally failing to keep pace with sea-level rise, and may be on the precipice of drowning. Similar projections of interior deterioration and/or drowning have been made through numerical modeling[44,45] and validated through some limited field and remote-sensing data[46–48], including observations of the enlargement of interior channels at Sapelo Island[49].

Together, these findings reveal that, even in sandier barrier systems of the southeastern USA, those marshes capable of receiving sediment delivered through wave suspension (i.e., highly exposed and edge-proximal marshes) are far more resilient than those in more interior and protected settings. This aligns with modeling outcomes demonstrating that overall sediment availability may not preclude internal fragmentation if mineral delivery to the interior is constrained by limited inundation and/or sediment trapping at the periphery[50–52]; this study thus extends those findings to mesotidal settings. It further adds to the body of literature demonstrating the role of sedimentation—and of the storms which are largely responsible for sediment delivery[53]—in marsh survival. This process may be exacerbated along barrier-associated marshes such as those of the Southeast USA: here, continued decreases in sediment inputs to these backbarriers and coastal ocean from local rivers[54] may hasten fragmentation, resulting in persistence of only those exposed, edge-proximal marshes which today show no such signs of imminent threat. The resulting apparent trend is one of rapid fragmentation, converting broad platform marshes to doughnut-like configurations in which marsh peripheries continue to grow apace with RSLR, while marsh interiors drown and convert to open water. Given the outsized role that marshes play in the stability of fronting barrier islands[55], this fragmentation threatens the overall health of the broader barrier systems studied here, as well as similar backbarrier marshes globally.

Methods

Sediment core collection. Long-term (50–100 years) vertical accretion rates were determined from sediment cores collected in December 2017 along transects from the mainland to fronting barrier islands at four barrier systems in the Georgia Bight (Fig. 1): the Cape Romain cuspate foreland (north-central South Carolina), Hilton Head (southern South Carolina), Sapelo Island (central Georgia), and Amelia Island (northern Florida). Two cores were collected along each transect at sampling stations located approximately one-third and two-thirds of the distance between the mainland and fronting barrier island. Cores were collected ~10 m from the marsh edge and landward of any visible topographic high (marsh levee), and in marshes at the boundary between short- (stunted) and tall-form *S. alterniflora* (as described by ref. [56]), which locally are roughly 25–40 cm and 90–140 cm in height, respectively. Station locations were described in the field, including primary and secondary vegetation, presence of proximal (within ~100 m) marsh pools and tidal creeks, and other physical characteristics. Cores were collected using a metal corer 15.3-cm in diameter, 80 cm in length, and with sharpened cutting head, and extruded into protective PVC casings. The elevation of marsh within the cores were compared with ambient adjacent marsh prior to ground extraction to ensure the peat/sediment within the core did not undergo any compaction during coring.

Supplementary marsh samples were collected adjacent to accretion cores using a Russian peat borer, penetrating to at least 40 cm. At least 15, 1-cm thick samples from each core were collected, treated with hydrogen peroxide to remove organic matter, and analyzed using a Beckman-Coulter® (Brea, California, USA) Laser Diffraction Particle Size Analyzer. Resulting sand:-mud ratios averaged from each of our four barrier systems are given in Supplementary Table 1. More comprehensive data and analyses are presented by Staro et al. (ref. [57]).

Elevations for each core were recorded relative to North American Vertical Datum (m NADV88, ±2 cm) using a Topcon Hiper Lite II global positioning system with integrated real-time kinematics (RTK-GPS), and corrected with the National Oceanic and Atmospheric Administration (NOAA) Online Positioning User Service (OPUS) These were converted to elevations with respect to mean tidal level (m MTL) using the National Oceanographic and Atmospheric Administration (NOAA) Online Vertical Datum Transformation (VDatum) system. We

then normalized these elevations (Z) to the local tidal range estimated from nearby tide gauges through calculation for each site of Z^*_{MHW} values following Holmquist and Windham-Myers[58]:

$$Z^*_{MHW} = (Z - MSL)/(MHW - MSL) \quad (1)$$

in which MSL is the elevation of local mean sea level and MHW is the elevation of local mean high water.

Sapelo Island is located approximately equidistant between tide gauges at Fernandina Beach and Fort Pulaski. For this site, $RSLR_C$ (contemporaneous relative sea level rise, defined below in *Normalization of Accretion Rates*) values were calculated by averaging sea-level-rise rates for the given time period from these two gauges. We did the same for sites in our database for the Charleston and Myrtle Beach (Springmaid Pier, SC) tide gauges for sites located approximately equidistant between those gauges (all sites north of Cape Romain).

Determination of marsh accretion rates. Marsh cores were split lengthwise, described, and photographed. They were then sectioned at 1-cm intervals in the top 6 cm, 2-cm intervals from 6 to 30 cm depth, and then 5-cm intervals to the bottom of the core (between 35 and 65 cm depth, depending on the total core length). This approach allows for higher-resolution sampling in shallow sections of the core which will contain the highest, and most rapidly changing ^{210}Pb contents. Cut rounds (1–5 cm thick; ~150–900 cm^3) of each sample ($n = 360$; average of 22–23 samples/core) were analyzed for both wet and dry bulk density by weighing, drying for 24 h in a 60 °C oven, and re-weighing. Total organic-matter content was determined from aliquots (~1–3 g) of dry sample rounds by loss-on-ignition[59] through furnace combustion for 14 h at a temperature of 650 °C. The remaining raw material from each sample was analyzed for radioactive ^{210}Pb and ^{137}Cs contents using gamma-ray spectroscopy. Radioactive ^{210}Pb is a naturally occurring nuclide of the ^{238}U series formed from the decay of ^{222}Rn gas[60]. It is constantly replenished in the atmosphere and is quickly incorporated into water, soils, and sediment at the Earth's surface, where it undergoes beta decay (with attendant emission of a quantum of gamma radiation) with a half-life of 22.3 years[60]. In contrast, ^{137}Cs is an anthropogenic fallout nuclide, predominantly produced during the period of extensive atmospheric thermonuclear testing between the mid-1940s and mid-1970s; peak ^{137}Cs fallout occurred in 1963–1964, with a gradual decline interrupted by fallout events such as the 1986 Chernobyl disaster[61].

Sediments from each sample were homogenized, massed, packed into petri dishes of known geometries (40 or 70 mL), sealed using vinyl electrical tape and paraffin wax, and stored for at least 30 days to ensure equilibrium between ^{226}Ra and its daughter products ^{214}Pb and ^{214}Bi. Samples were then analyzed for standard-adjusted ^{137}Cs (662.6 keV photopeak), ^{210}Pb (46.5 keV photopeak), ^{214}Pb (295, 352 keV photopeaks), and ^{214}Bi (609 keV photopeak) activity (reported in disintegrations per minute per gram [dpm/g]) using shielded, ultra-low background Canberra Low Energy Germanium (LEGe) or Broad Energy Germanium (BEGe) detectors for a period of 24 hours. Following corrections for sample-depth attenuations, total ^{137}Cs and each of total ^{210}Pb, supported ^{210}Pb (that produced in situ from the decay of ^{226}Ra, a naturally occurring radioisotope found in most rocks and soils), and unsupported (excess) ^{210}Pb ($^{210}Pb_{xs}$) concentrations were calculated for each sample and converted to units of Bq/kg. The atmospherically deposited $^{210}Pb_{xs}$ is calculated by subtracting supported ^{210}Pb from total ^{210}Pb activity for each sample.

Following Appleby[60] and Corbett and Walsh[62], marsh ^{210}Pb-based accretion rates were calculated using the Constant Flux and Constant Sedimentation (CFCS) model originally devised by Krishnaswamy[63]. This assumes a constant accumulation rate (both inorganic and organic sedimentation) and constant flux of ^{210}Pb to the marsh surface. The accretion rate (S) is calculated as

$$S = \lambda/m \quad (2)$$

in which λ is the decay constant for ^{210}Pb (0.03114 yr^{-1}) and m is the slope of the regression between depth and the natural log of $^{210}Pb_{xs}$ activity of each sample between the surface and the depth at which total ^{210}Pb activity reaches background (supported) levels (i.e., $^{210}Pb_{xs} = 0$). Obvious outliers—including those associated with any surface mixed layer—were removed from the analysis (Supplementary Figs. 1–4). Rate uncertainties are calculated as the standard deviation of rates determined via sensitivity analysis through progressive removal of single data points from the down-core profile and re-calculation of the core-average rate. Accretion rates determined from the CFCS-based $^{210}Pb_{xs}$ models are verified against those independently determined from peak down-core concentrations of ^{137}Cs (corresponding to 1964 C.E.). As accretion rates determined from ^{137}Cs are based on the depth of single samples (i.e., those with first occurrence or peak of ^{137}Cs), the associated rate uncertainties simply reflect sample thickness.

Normalization of accretion rates. Following Saintilan et al. [23], for each core, we calculated the "Contemporaneous Relative Sea-Level Rise" rate ($RSLR_C$); that is, the rate of RSLR over the calculated period of accretion based on the $^{210}Pb_{xs}$CFCS rate. For example, for a core for which the upper-most 40 cm were used to determine a $^{210}Pb_{xs}$CFCS rate of 5 mm yr^{-1}, the period of time captured by that accretion rate would be 80 years. The $RSLR_C$ rate is calculated by linear regression of monthly sea-level values from the nearest tide gauge (Supplementary Table 1) for the period December 1937 – December 2017 (80 years previous till the date of core collection). Sapelo Island is located approximately equidistant between tide gauges at Fernandina Beach and Fort Pulaski. For this site, $RSLR_C$ values were calculated by averaging sea-level-rise rates for the given time period from these two gauges. We did the same for sites in our database for the Charleston and Myrtle Beach (Springmaid Pier, SC) tide gauges for sites located approximately equidistant between those gauges (all sites north of Cape Romain). For cores containing a surface mixed layer (identified as a vertical $^{210}Pb_{xs}$ profile, such as that observed in core HH-T1S2; Supplementary Fig. 2), we assumed a constant accretion rate from the top-most sample included in our CFCS calculation to the surface.

For each core we then define the dimensionless 'Contemporaneous Accretion Excess' (AE_C) as

$$AE_C = {}^{210}Pb_{xs}CFCS\,(mm\,yr^{-1})/RSLR_C\,(mm\,yr^{-1}) \quad (3)$$

Marshes with AE_C values equal to 1 have been accreting at the same rate as RSLR over the time period for which accretion is measured. An AE_C value of <1 indicates a marsh is failing to keep pace with sea-level rise, whereas $AE_C > 1$ denotes vertical accretion outpacing RSLR. Errors for AE_C are propagated from $^{210}Pb_{xs}$CFCS and $RSLR_C$ uncertainties for each core. Recognizing that marshes may not respond instantaneously to a change in the rate of sea-level rise[64,65], we also determine in the same manner the RSLR rate over the 50-year period prior to core collection ($RSLR_{50}$). This follows the approach of Saintilan et al. [23], who, in comparing only SET/MH-derived sedimentation rates determined from 477 monitoring stations across four continents, found that $RSLR_{50}$ was the most important predictor of the rate of vertical accretion. This was

particularly true for organic-rich marshes, suggesting a lagged marsh response to an increase in the rate of RSLR, and thus potential marsh resilience to accelerated sea-level rise. We therefore calculate the Accretion Excess in comparison to this long-term RSLR rate (the 'AE_{50}') according to Eq. (3), substituting $RSLR_{50}$ for $RSLR_C$. Errors are propagated in the same manner as for AE_C.

We note that for six of our cores (CR-T1S2, CR-T2S4, HH-T1S2, HH-T1S4, HH-T2S2, and AI-T1S3) we omitted from our accretion calculations surface sediments <10 cm thick which showed disturbance in $^{210}Pb_{xs}$ profiles (Supplementary Figs. 1–4). For these we simply propagated the same accretion rate to the core surface (i.e., assumed that the marsh accreted at that same rate until 2017 as it had for the period [depth] from which the accretion rate was calculated) for purposes of calculating $RSLR_C$ and $RSLR_{50}$. As the upper 4–10 cm of sample for these cores was not used in accretion calculations, this approach provides a conservative (low-end) estimate of marsh accretion: that upper marsh grew most recently (the ~10–25 years prior to 2017), and thus under conditions of higher sea-level rise than the earlier period for which data allowed determination of marsh accretion.

Development of regional Database. We developed a regional database of marsh accretion for the Georgia Bight, updating that presented by Crotty et al. [66] and incorporating data from our 16 new cores (Supplementary Data 1). This updated database includes those accretion rates reported by Alexander et al.[67], Crotty et al.[66], Goldberg et al.[68], Langston et al.[26], Loomis and Craft[69], Morris et al.[9], Raposa et al.[7], Sharma et al.[70], Vogel et al.[71], and Weston et al.[8]. Marsh accretion rates in this database were determined through a combination of ^{210}Pb and/or ^{137}Cs measurements, SETs, and MHs. For each of these, we compiled available elevation, accretion, and site-characteristic data. Where not reported, we apply an accretion rate uncertainty equal to our study-average ±3% and ±6% to all reported ^{210}Pb and ^{137}Cs rates, respectively. For SET and MH rates, we apply an uncertainty equal to 0.10 mm yr^{-1}. Elevation transformations to Z^*_{MHW}, determination of $RSLR_C$, and calculation of AE_C and AE_{50} values for each of these marsh accretion stations were conducted in the same manner as described above for our cores. In (very common) cases in which down-core ^{210}Pb values are not provided in published data, we are unable to determine time periods associated with resulting ^{210}Pb-derived accretion rates; hence, for these we can assign neither $RSLR_C$ nor AE_C values. However, as long as a core collection date is provided, $RSLR_{50}$ nor AE_{50} values are calculated.

Of the resulting combined 103 marsh accretion measurements, we exclude or partially exclude seven from further analysis (see final column of Supplementary Data 1). This includes three sites fully omitted for which the measurement record was <5 years. For example, ^{210}Pb results from core GCE5_C8 of Langston et al. [26] (who also omitted this core) have a reported accretion rate of ~290 mm yr^{-1}, resulting in an accretion period for the measured core of <2 years. From an additional site (Goat Island SET record; from ref. [9]) we incorporate the accretion rate and AE_{50} value, but omit the AE_C value because calculated sea-level change over the brief study period (1997–2002) was negative (−6.5 mm yr^{-1}). The final three partially omitted records are from the robust database from the Georgia Coastal Ecosystems Long Term Ecological Research site (located within the backbarrier of Sapelo Island), presented by Langston et al. [26]. Of their 20 reported ^{210}Pb accretion rates, the down-core ^{210}Pb data from three sites (GCE4_C4, GCE5_C4, GCE5_C9) show thick surface mixed layers, leading to substantial uncertainty in the start year for the accretion analysis (or, if the calculated rate is applied to the whole core, including the mixed layer [as we did for our analysis], the result is an unrealistically old record given the ~100-year age range of ^{210}Pb). For these, we incorporate the resulting accretion rate into our analysis, but do not calculate AE_C or AE_{50} values, as we cannot determine the time period captured by their records and thus the associated $RSLR_C$ or $RSLR_{50}$ rates.

Reporting summary. Further information on research design is available in the Nature Portfolio Reporting Summary linked to this article.

Data availability

Data associated with this manuscript includes new down-core ^{210}Pb, ^{137}Cs, bulk density, and loss-on-ignition data for 16 new marsh sediment cores, and associated calculated $^{210}Pb_{xs}$CFCS and ^{137}Cs accretion rates; down-core averaged bulk density and loss-on-ignition values; and calculated $RSLR_{50}$, $RSLR_C$, AE_C, and AE_{50} values for these new cores and for those marsh accretion and/or sedimentation rates included in our regional compilation. All core-average and compiled and calculated data associated with this manuscript, including all shown in all figures and tables, are available in Supplementary Data 1. The full dataset, including down-core data for our new cores, is available at https://doi.org/10.25921/eff9-d732.

Received: 16 June 2023; Accepted: 12 January 2024;
Published online: 09 February 2024

References

1. Redfield, A. C. Development of a New England salt marsh. *Ecol. Monogr.* **42**, 201–237 (1972).
2. Nyman, J. A., DeLaune, R. D., Roberts, H. H. & Patrick, W. H. Jr Relationship between vegetation and soil formation in a rapidly submerging coastal marsh. *Mar. Ecol. Prog. Ser.* **96**, 269–279 (1993).
3. Cahoon, D. R., Lynch, J. C., Roman, C. T., Schmit, J. P. & Skidds, D. E. Evaluating the relationship among wetland vertical development, elevation capital, sea-level rise, and tidal marsh sustainability. *Estuaries Coast* **42**, 1–15 (2019).
4. Reed, D. J. The impact of sea-level rise on coastal salt marshes. *Prog. Phys. Geogr.* **14**, 465–481 (1990).
5. Cahoon, D. R. & Reed, D. J. Relationships among marsh surface topography, hydroperiod, and soil accretion in a deteriorating Louisiana salt marsh. *J. Coast. Res.* **11**, 357–369 (1995).
6. Kirwan, M. L. et al. Limits on the adaptability of coastal marshes to rising sea level. *Geophys. Res. Lett.* **37**, https://doi.org/10.1029/2010GL045489 (2010).
7. Raposa, R. B. et al. Assessing tidal marsh resilience to sea-level rise at broad geographic scales with multi-metric indices. *Biol. Conserv.* **204**, 263–275 (2016).
8. Weston, N. B. et al. Recent acceleration of wetland accretion and carbon accumulation along the US East Coast. *Earth's Future* **11**, e2022EF003037 (2023).
9. Morris, J. T., Sundareshwar, P. V., Nietch, C. T., Kjerfve, B. & Cahoon, D. R. Responses of coastal wetlands to rising sea level. *Ecology* **83**, 2869–2877 (2002).
10. Kirwan, M. L. & Mudd, S. M. Response of salt-marsh carbon accumulation to climate change. *Nature* **489**, 550–553 (2012).
11. Langley, J. A., McKee, K. L., Cahoon, D. R., Cherry, J. A. & Megonigal, J. P. Elevated CO_2 stimulates marsh elevation gain, counterbalancing sea-level rise. *Proc. Natl. Acad. Sci. USA* **106**, 6182–6186 (2009).
12. Ratliff, K. M., Braswell, A. E. & Marani, M. Spatial response of coastal marshes to increased atmospheric CO_2. *Proc. Natl. Acad. Sci. USA* **112**, 15580–15584 (2015).
13. McKee, K. L. & Cherry, J. A. Hurricane Katrina sediment slowed elevation loss in subsiding brackish marshes of the Mississippi River delta. *Wetlands* **29**, 2–15 (2009).
14. Baustian, J. J. & Mendelssohn, I. A. Hurricane-induced sedimentation improves marsh resilience and vegetation vigor under high rates of relative sea level rise. *Wetlands* **35**, 795–802 (2015).
15. Zhu, Q. & Wiberg, P. L. The importance of storm surge for sediment delivery to microtidal marshes. *J. Geophys. Res. Earth Surf* **127**, e2022JF006612 (2022).
16. Bricker-Urso, S., Nixon, S. W., Cochran, J. K., Hirschberg, D. J. & Hunt, C. Accretion rates and sediment accumulation in Rhode Island salt marshes. *Estuaries* **12**, 300–317 (1989).
17. Weston, N. B. Declining sediments and rising seas: an unfortunate convergence for tidal wetlands. *Estuaries Coast.* **37**, 1–23 (2014).

18. FitzGerald, D. M. et al. Largest marsh in New England near a precipice. *Geomorphology* **379**, 107625 (2021).
19. Crosby, S. C. et al. Spartina alterniflora biomass allocation and temperature: implications for salt marsh persistence with sea-level rise. *Estuaries Coast* **40**, 213–223 (2017).
20. Cahoon, D. R. A review of major storm impacts on coastal wetland elevations. *Estuaries Coasts* **29**, 889–898 (2006).
21. Morton, R. A. & Barras, J. A. Hurricane impacts on coastal wetlands: a half-century record of storm-generated features from southern Louisiana. *J. Coast. Res* **27**, 27–43 (2011).
22. Holmquist, J. R., Brown, L. N. & MacDonald, G. M. Localized scenarios and latitudinal patterns of vertical and lateral resilience of tidal marshes to sea-level rise in the contiguous United States. *Earth's Future* **9**, e2020EF001804 (2021).
23. Saintilan, N. et al. Constraints on the adjustment of tidal marshes to accelerating sea level rise. *Science* **377**, 523–527 (2022).
24. Kirwan, M. L. & Megonigal, J. P. Tidal wetland stability in the face of human impacts and sea-level rise. *Nature* **504**, 53–60 (2013).
25. Hayes, M. O. The Georgia bight barrier system in *Geology of Holocene Barrier Island Systems* (ed. Davis, R. A. Jr) 233–304 (Springer, 1994).
26. Langston, A. K., Alexander, C. R., Alber, M. & Kirwan, M. L. Beyond 2100: elevation capital disguises salt marsh vulnerability to sea-level rise in Georgia, USA. *Estuar Coast. Shelf Sci* **249**, 107093 (2021).
27. Breithaupt, J. L. et al. Avoiding timescale bias in assessments of coastal wetland vertical change. *Limnol. Oceanogr.* **63**, S477–S495 (2018).
28. Valentine, K. & Mariotti, G. Wind-driven water level fluctuations drive marsh edge erosion variability in microtidal coastal bays. *Cont. Shelf Res.* **176**, 76–89 (2019).
29. Cortese, L. & Fagherazzi, S. Fetch and distance from the bay control accretion and erosion patterns in Terrebonne marshes (Louisiana, USA). *Earth Surf Process Landf* **47**, 1455–1465 (2022).
30. Temmerman, S., Govers, G., Wartel, S. & Meire, P. Spatial and temporal factors controlling short-term sedimentation in a salt and freshwater tidal marsh, Scheldt estuary, Belgium, SW Netherlands. *Earth Surf Process. Landf.* **28**, 739–755 (2003).
31. Ganju, N. K. et al. Sediment transport-based metrics of wetland stability. *Geophys. Res. Lett.* **42**, 7992–8000 (2015).
32. Puchkoff, A. L. & Lawrence, B. A. Experimental sediment addition in salt-marsh management: Plant-soil carbon dynamics in southern New England. *Ecol. Eng.* **175**, 106495 (2022).
33. Zoccarato, C. et al. In-situ loading experiments reveal how the subsurface affects coastal marsh survival. *Commun. Earth Environ.* **3**, 1–12 (2022).
34. McCloskey, T. A., Smith, C. G., Liu, K. B. & Nelson, P. R. The effects of tropical cyclone-generated deposition on the sustainability of the Pearl River Marsh, Louisiana: The importance of the geologic framework. *Front. Ecol. Evol.* **6**, 179 (2018).
35. Schuerch, M., Spencer, T. & Evans, B. Coupling between tidal mudflats and salt marshes affects marsh morphology. *Mar. Geol.* **412**, 95–106 (2019).
36. Hopkinson, C. S., Morris, J. T., Fagherazzi, S., Wollheim, W. M. & Raymond, P. A. Lateral marsh edge erosion as a source of sediments for vertical marsh accretion. *J. Geophys. Res. Biogeosci.* **123**, 2444–2465 (2018).
37. Castagno, K. A. et al. Intense storms increase the stability of tidal bays. *Geophys. Res. Lett.* **45**, 5491–5500 (2018).
38. Staro, A. et al. Hurricane deposition can enhance salt marsh resiliency to sea-level rise in *American Geophysical Union Fall Meeting Abstracts*, EP13A-02 (2021).
39. Mariotti, G., Kearney, W. S. & Fagherazzi, S. Soil creep in salt marshes. *Geology* **44**, 459–462 (2016).
40. Tognin, D., D'Alpaos, A., Marani, M. & Carniello, L. Marsh resilience to sea-level rise reduced by storm-surge barriers in the Venice Lagoon. *Nat. Geosci.* **14**, 906–911 (2021).
41. Yando, E. S. et al. An integrative salt marsh conceptual framework for global comparisons. *Limnol. Oceanogr. Lett.* 1–20 https://doi.org/10.1002/lol2.10346 (2023).
42. Marani, M., D'Alpaos, A., Lanzoni, S. & Santalucia, M. Understanding and predicting wave erosion of marsh edges. *Geophys. Res. Lett.* **38**, L21401 (2011).
43. Mariotti, G. & Fagherazzi, S. Critical width of tidal flats triggers marsh collapse in the absence of sea-level rise. *Proc. Natl Acad. Sci. USA* **110**, 5353–5356 (2013).
44. Fagherazzi, S., *et al* Numerical models of salt marsh evolution: Ecological, geomorphic, and climatic factors. *Rev. Geophys.* **50** (2012).
45. Mariotti, G. Beyond marsh drowning: the many faces of marsh loss (and gain). *Adv. Water Resources* **144**, 103710 (2020).
46. Couvillion, B. R. Land area in coastal Louisiana (1932 to 2016): land area spatial data-multi-date composites for specific years: US Geological Survey data release (2018).
47. Ortiz, A. C., Roy, S. & Edmonds, D. A. Land loss by pond expansion on the Mississippi River Delta Plain. *Geophys. Res. Lett.* **44**, 3635–3642 (2017).
48. Schepers, L., Kirwan, M. L., Guntenspergen, G. & Temmerman, S. Spatio-temporal development of vegetation die-off in a submerging coastal marsh. *Limnol. Oceanogr.* **62**, 137–150 (2017).
49. Burns, C. J., Alber, M. & Alexander, C. R. Historical changes in the vegetated area of salt marshes. *Estuaries Coast* **44**, 162–177 (2021).
50. D'Alpaos, A. & Marani, M. Reading the signatures of biologic–geomorphic feedbacks in salt-marsh landscapes. *Adv. Water Resources* **93**, 265–275 (2016).
51. Zhang, X., Leonardi, N., Donatelli, C. & Fagherazzi, S. Fate of cohesive sediments in a marsh-dominated estuary. *Adv. Water Resources* **125**, 32–40 (2019).
52. Vinent, O. D., Herbert, E. R., Coleman, D. J., Himmelstein, J. D. & Kirwan, M. L. Onset of runaway fragmentation of salt marshes. *One Earth* **4**, 506–516 (2021).
53. Turner, R. E., Baustian, J. J., Swenson, E. M. & Spicer, J. S. Wetland sedimentation from hurricanes Katrina and Rita. *Science* **314**, 449–452 (2006).
54. Windom, H. L. & Palmer, J. D. Changing river discharge and suspended sediment transport to the georgia bight: implications to saltmarsh sustainability. *J. Coast Res* **38**, 512–522 (2022).
55. FitzGerald, D. M. et al. In *Barrier Dynamics and Response to Changing Climate* (eds. Moore, L. J. & Murray, A. B.) 3–56 (Springer, 2018).
56. Gallagher, J. L., Somers, G. F., Grant, D. M. & Seliskar, D. M. Persistent differences in two forms of Spartina alterniflora: a common garden experiment. *Ecology* **69**, 1005–1008 (1988).
57. Staro, A. et al. Hurricane deposition can enhance salt marsh resiliency to sea-level rise. *AGU Fall Meeting Abstracts* **2021**, EP13A-02 (2021).
58. Holmquist, J. R. & Windham-Myers, L. A conterminous USA-scale map of relative tidal marsh elevation. *Est. Coast.* **45**, 1596–1614 (2022).
59. Dean, W. E. Determination of carbonate and organic matter in calcareous sediments and sedimentary rocks by loss on ignition; comparison with other methods. *J. Sed. Res.* **44**, 242–248 (1974).
60. Appleby, P. G. In *Tracking Environmental Change Using Lake Sediments* (eds. Last, W. M. & Smol, J. P.) (Springer, 2001).
61. Walling, D. E., He, Q. & Quine, T. A. In: *Proc. International Symposium held at Boulder, Colorado, USA, During the XXI General Assembly of Geodesy and Geophysics* 163–172 (IAHS Press, 1995).
62. Corbett, D. R. & Walsh, J. P. In *Handbook of Sea-level Research* (eds. Shennan, I., Long, A. J. & Horton, B. P.) 361–372 (John Wiley & Sons, 2015).
63. Krishnaswamy, S., Lal, D., Martin, J. M. & Meybeck, M. Geochronology of lake sediments. *Earth Planet. Sci. Lett.* **11**, 407–414 (1971).
64. Kirwan, M. L. & Murray, A. B. Tidal marshes as disequilibrium landscapes? Lags between morphology and Holocene sea level change. *Geophys. Res. Lett.* **35** https://doi.org/10.1029/2008GL036050 (2008).
65. Kolker, A. S., Goodbred, S. L. Jr, Hameed, S. & Cochran, J. K. High-resolution records of the response of coastal wetland systems to long-term and short-term sea-level variability. *Estuar. Coast. Shelf Sci.* **84**, 493–508 (2009).
66. Crotty, S. M. et al. Sea-level rise and the emergence of a keystone grazer alter the geomorphic evolution and ecology of southeast US salt marshes. *Proc. Natl Acad. Sci. USA* **117**, 17891–17902 (2020).
67. Alexander, C. R., Hodgson, J. Y. S. & Brandes, J. A. Sedimentary processes and products in a mesotidal salt marsh environment: insights from Groves Creek, Georgia. *Geo-Marine Lett.* **37**, 345–359 (2017).
68. Goldberg, E. D., Griffin, J. J., Hodge, V., Koide, M. & Windom, H. Pollution history of the Savannah River estuary. *Environ. Sci. Technol.* **13**, 588–594 (1979).
69. Loomis, M. J. & Craft, C. B. Carbon sequestration and nutrient (nitrogen, phosphorus) accumulation in river-dominated tidal marshes, Georgia, USA. *Soil Sci. Soc. Am. J.* **74**, 1028–1036 (2010).
70. Sharma, P., Gardner, L. R., Moore, W. S. & Bollinger, M. S. Sedimentation and bioturbation in a salt marsh as revealed by ^{210}Pb, ^{137}Cs, and ^{7}Be studies. *Limnol. Oceanogr.* **32**, 313–326 (1987).
71. Vogel, R. L., Kjerfve, B. & Gardner, L. R. Inorganic sediment budget for the North Inlet salt marsh, South Carolina, USA. *Mangroves Salt Marshes* **1**, 23–35 (1996).

Acknowledgements

Funding for this study was provided by the National Science Foundation Geomorphology and Land Use Dynamics Program (award numbers EAR-1800825 [RAPID], EAR-1904496 [RAPID], and EAR-2022987). The authors thank Tara Yocum and Michael Brown (University of New Orleans) for assistance with field sampling logistics and Elizabeth Davis (Virginia Institute of Marine Science) for guidance with data analysis. Portions of this study are derived from the William & Mary senior thesis of K.K. who was supported by the Geology Department for this work. This work is a contribution to IGCP Project 725 'Forecasting Coastal Change'.

Author contributions

C.J.H., D.M.F., Z.J.H., and I.Y.G. conceptualized and designed the study, and obtained the funding. J.E.C. and K.K. conducted all laboratory analyses, with advising from C.J.H. J.E.C., and C.J.H. conducted all data analysis. C.J.H. led manuscript preparation and drafted all figures, with contributions from all co-authors.

Competing interests

The authors declare that the research was conducted in the absence of any commercial or financial relationships that could be construed as a potential competing interest.

Additional information

Supplementary information The online version contains supplementary material available at https://doi.org/10.1038/s43247-024-01219-8.

Correspondence and requests for materials should be addressed to Christopher J. Hein.

Peer review information *Communications Earth & Environment* thanks Elena Solohin and the other, anonymous, reviewer(s) for their contribution to the peer review of this work. Primary Handling Editors: Helen McGregor and Clare Davis. A peer review file is available.